*Optica Applicata, Vol. XVII, No. 4, 1987*

# Multichannel grating phase-stepped interferometers

MAŁGORZATA KUJAWIŃSKA

Warsaw University of Technology, Institute of Design of Precise and Optical Instruments, ul. Karola Chodkiewicza 8, 02–525 Warszawa, Poland.

New applications of three- and fourchannel phase-stepped interferometers have been presented whereby automatic fringe analysis in grating interferometer can be performed when recording transient events. The theory is developed and the analysis of the sources of error are presented with the aid of computer simulations. The main problems connected with the analysis in fourchannel interferometer are discussed. The adjustment procedure and initial experimental results are shown to confirm the utility of the systems.

## 1. Introduction

Interferometry and holographic interferometry are becoming useful tools for precision measurements in research and industrial applications. In recent years computer analysis is of increasing importance in interferometry [1]. The use of solid-state detector arrays, image memory boards together with microprocessors and computers for the extraction of the information from the interferograms and high resolution graphic boards find important application in optical metrology.

Automated quantitative evaluation of interferograms requires accurate interference phase measurement, independent of fringe position and intensity variation superposed onto the interferograms. The different methods of fringe pattern analysis can be classified into static and dynamic methods [2].

For static methods, closed fringes should be avoided, hence a tilt needs frequently to be introduced. Fringe contours can be extracted manually or by digitizing fringe center with manual digitizer or densitometer. Video-techniques and image processing can be obtained by symmetrically coding fringes to a skeleton in a treshold version of the interferogram. Also a phase detection technique in the spatial domain using Fourier transform method or 2–D Fourier analysis in connection with video-technique can be used. In Fourier methods the information content of interferogram is limited as it has to be filtered in the spatial domain.

In dynamic methods the relative phase between the reference beam and the test beam in a two-beam arrangement is varied at constant, controlled rate (heterodyne technique) or in steps of $\pi/2$ for instance (quasi-heterodyne or phase-stepping techniques). In the heterodyne method the interference phase is measured electrically from the beat signal between the two interfering beams. Heterodyne interferometry offers high spatial resolution and interpolation up to 1/1000 of a fringe. It requires, however, sophisticated electronic equipment and mechanical scanning of the fringe

pattern. In the phase-stepping technique the relative phase is changed continuously or stepwise, using at least three phase shifts of 90 or 120 degrees. The phase of the interference patterns can then be computed from the intensity values measured. The phase stepping technique is very appropriate for digital processing and TV techniques and leads to sensitivity of 1/100 of a fringe at any of the fringe pattern in the TV image.

The static techniques enable the automatic interferogram analysis of dynamic processes, however, the fringe patterns should be of suitable form for fringe tracing or Fourier transform method [3].

The dynamic techniques are not suitable for the analysis of transient events, as they require time for recording of at least three separate interferograms or mechanical scanning of the fringe pattern.

Lately, a remarkably simple approach using a linear grating has been found to be useful for phase stepping in different types of interferometers [4]. Simple diffraction gratings have been used to produce phase-shifted interferograms instantaneously for the measurement of any wavefront using charge-couple device (CCD) array detectors. The analysis of instantaneously produced three or four interferograms enable quick and comfortable analysis of transient events and reduces the sensitivity of the interferometer to fluctuations of environmental parameters (temperature, illumination drift etc.). However, some additional sources of error appear in multichannel interferometers. The threechannel interferometer suffers mainly due to the fact that the data are collected from different parts of a detector and the interferograms are produced by different diffraction order beams. The fourchannel crossed-grating interferometer supplies the information about two functions ($\partial\Phi/\partial x$ and $\partial\Phi/\partial y$, where $\Phi$ is the wavefront phase function). Herein the phase fringes of the first function calculated from four interferograms break through into the phase fringes of the second function. This phenomena due to a small number of measurements is emphasized by different sources of error in the setup. Therefore the ambiguous areas in wrapped phase functions may occur and the fringe counting process may produce some error in the unwrapped phase.

The principle and basic arrangements of three- and fourchannel interferometers are described and the detailed analysis of systematic and statistic errors is given. The modified processing procedure for fringe pattern analysis and the results of experiments are presented.

## 2. Principle of a threechannel phase-stepped interferometer

The intensity distribution of an interference pattern can be written at each detector point as

$$I(x, y) = a(x, y) + b(x, y)\cos[\Phi(x, y) + \delta] \tag{1}$$

where: $a(x, y)$ and $b(x, y)$ are the background level and fringe modulation function, respectively; $\Phi(x, y)$ is the wavefront phase, $\delta$ is an arbitrary constant phase difference between the object and references beams.

One method of solving Eq. (1) is based on a three phase stepping technique [5]. By adding a known phase shift to the reference or object beam of the interferometer Eq. (1) becomes

$$I(x, y) = a(x, y) + b(x, y)\cos[\Phi(x, y) + k\delta] \tag{2}$$

where we assume $k = 0, \pm 1$. Herein we would like to obtain the three fringe patterns, corresponding to interferograms with different shift, simultaneously. If we introduce the linear, diffraction gratings into object and reference beams of an interferometer, it serves two important roles. The grating diffracts the beam into many diffracted beams. Also any translation motion or lateral shift of the grating with respect to the optical axis introduces additional phase terms into each of the diffracted beams.

The generalized transmission function of the grating with an arbitrary lateral translation $x_o$ introduced can be written as

$$T(x - x_o, y) = \Sigma\, c_k \exp i2\pi k\omega(x - x_o) \tag{3}$$

where: $c_k$ is the $k$-th coefficient of the one dimensional Fourier series of a linear grating ($k$ is integer), $\omega$ is the fundamental grating frequency, $x_o$ is the lateral translation of the grating, perpendicular to its grooves.

At the image plane, the Fourier transforming of Eq. (3) yields a series of phase shifted delta functions, where the magnitude of the shift is given by

$$\delta = 2\pi k\omega x_o. \tag{4}$$

Therefore, for phase-shifting interferometry, a simultaneous set of three interferograms (Fig. 1) can be obtained from $+1$, 0, $-1$ orders of the diffracted beams. For 120-deg phase shift, the amount of the lateral translation of the grating $x_o$ is

$$x_o = 1/3\omega, \quad \text{or} \quad d/3 \tag{5}$$

where $d = 1/\omega$ indicates the grating period.

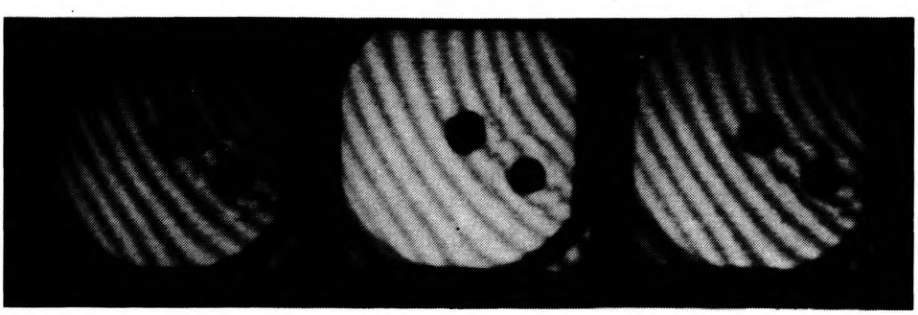

Fig. 1. Three phase shifted interferograms obtained in the grating holographic interferometer

The interferograms $I_0$, $I_{-1}$, $I_{+1}$ obtained by interference of the relevant diffracted beams are captured [5]. If we assume an equal diffraction efficiency in each of the orders, so that $a_k(x, y) = a(x, y)$ and $b_k(x, y) = b(x, y)$, the phase at a given point $(x, y)$

is given by equation

$$\Phi = \tan^{-1}\sqrt{3}(I_{+1}-I_{-1})/(2I_0-I_{+1}+I_{-1}). \tag{6}$$

The application of this principle had been demonstrated using the following interferometers: the point diffraction interferometer, the radial shear (Mach–Zechnder and triangular type) interferometer [4] and later the grating holographic interfometer [5].

The interferometers should fullfil three main, additional conditions connected with the phase-stepped technique applied in the systems. The spatial frequency of the grating should be sufficient to ensure the frequency separation of the pupils obtained for different diffraction orders. The high quality grating with near equal diffraction efficiency in the orders $+1$, 0, $-1$ should be used and the geometry of the set-up should ensure the required magnification and localization of the image of the fringe patterns in the plane of the detector.

The analysis of the errors which occur in this type of interferometers is presented in Section 5.1.

## 3. Principle of fourchannel phase-stepped interferometers

The principle of the phase-shifting interferometry combined with the fundamental characteristic of gratings may be also used in the crossed-grating lateral-shear interferometer or the crossed-grating holographic interferometer.

In 1973 WYANT [6] introduced holographically fabricated double-frequency crossed-grating lateral-shear interferometer to achieve two orthogonally lateral-sheared interferograms. The interferograms indicate the slope variations of the phase of the wavefront in the direction of lateral-shears and may be expressed by equations:

$$\begin{aligned} I_x(x, y) &= a(x, y)+b(x, y)\cos\left[\frac{\partial\Phi(x,y)}{\partial x}+\delta_x\right], \\ I_y(x, y) &= a(x, y)+b(x, y)\cos\left[\frac{\partial\Phi(x,y)}{\partial y}+\delta_y\right]. \end{aligned} \tag{7}$$

If we introduce a certain amount of phase shift into the four interferograms (indicated by numbers in Fig. 2) so that $\delta_x = \pm\Delta$ and $\delta_y = \pm\Delta$, we can generate four equations from relation (7) to represent the four phase-shifted interferograms:

$$\begin{aligned} A &= a+b\cos(\Phi_x-\Delta), \\ B &= a+b\cos(\Phi_x+\Delta), \\ C &= a+b\cos(\Phi_y-\Delta), \\ D &= a+b\cos(\Phi_y+\Delta) \end{aligned} \tag{8}$$

where $\Phi_x$ and $\Phi_y$ represent the first derivative of the phase (slope variations) in the $x$

and $y$ directions, respectively; $a$ and $b$ represent the background and fringe modulation functions. The capital letters indicate the intensity values at the given point $(x, y)$.

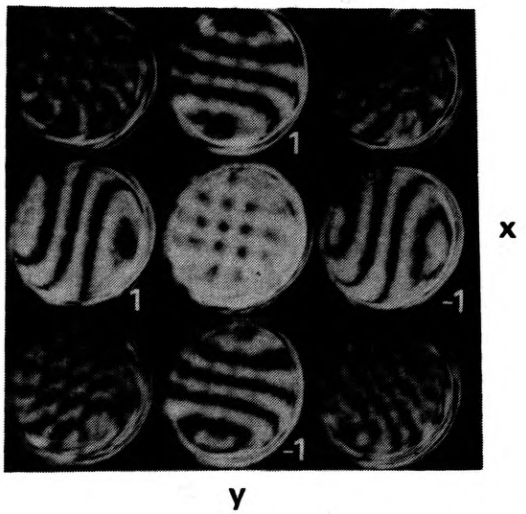


Fig. 2. Interferograms obtained in the double crossed-grating lateral-shear interferometer

If the phase shift introduced equals 45 deg the slope variations of the phase are described in the following equations:

$$\Phi_x = \tan^{-1}\frac{(A-B)(A+B)-(C+D)}{2AB-(A+B)(C+D)+(C^2+D^2)},$$
$$\Phi_y = \tan^{-1}\frac{(C-D)(C+D)-(A+B)}{2CD-(A+B)(C+D)+(A^2+B^2)}. \tag{9}$$

Let us consider the double crossed-grating lateral-shear interferometer as shown in Fig. 3. Two identical, parallel crossed-gratings are illuminated by a tested quasi-plane wavefront. The exact solution for the Fresnel field in the plane $IP$ may be obtained on the base of the analysis presented in [7] and [8].

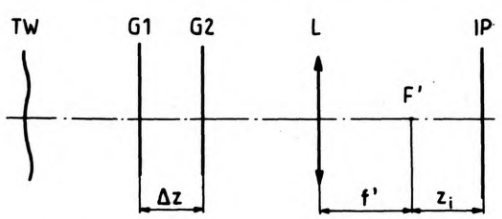


Fig. 3. Double crossed-grating interferometer. $TW$ – tested wavefront, $G1$, $G2$ – crossed-gratings, $L$ – imaging lens, $IP$ – image plane

If we consider the interference between the coincident wavefronts defined by the diffraction orders: (i) $m_{1x} = \pm 1$, $m_{2x} = 0$ and (ii) $m_{1x} = 0$, $m_{2x} = \pm 1$ for $x$-component grating and (i) $m_{1y} = \pm 1$, $m_{2y} = 0$ and (ii) $m_{1y} = 0$, $m_{2y} = \pm 1$ for $y$-component grating ($m_{1x/y}$, $m_{2x/y}$ are the diffraction orders in $x/y$ directions given by the first and second grating, respectively), four interferograms are obtained. They contain the

information about $\Phi_x$ and $\Phi_y$ slope functions. As it is shown in [8] the required phase shift in the fringe patterns may be obtained adjusting both: the in-plane translation of one of the gratings and the gap $\Delta z$ between the gratings. The resultant phase shifts for arbitrary position of the gratings and $m_1+m_2 = \pm 1$ diffraction orders in $x$ and $y$ directions equal, respectively:

$$\begin{aligned} \delta_{\pm 1x} &= P_{12}\omega \mp \omega x_o, \\ \delta_{\pm 1y} &= P_{12}\omega \mp \omega y_o, \end{aligned} \tag{10}$$

where $P_{12}$ is the constant proportional to the gap between the gratings and depending on the interferometer configuration, $x_o$ is the horizontal translation of the grating, $y_o$ is the vertical translation of the grating.

By introducing the in-plane translation $r$ of the grating in the 45 deg direction to the grooves of the grating we obtain the identical component translations in $x$ and $y$ directions ($x_o = y_o = r/\sqrt{2}$). The shift varies periodically as the gap changes. In order to obtain $\pm\delta$ phase shift in $\pm 1$ orders, the shift introduced by the gap should equal $2\pi K$ ($K$ is an integer), otherwise in influence $+1$ and $-1$ diffraction orders in a different way (as shown by Eq. (10)).

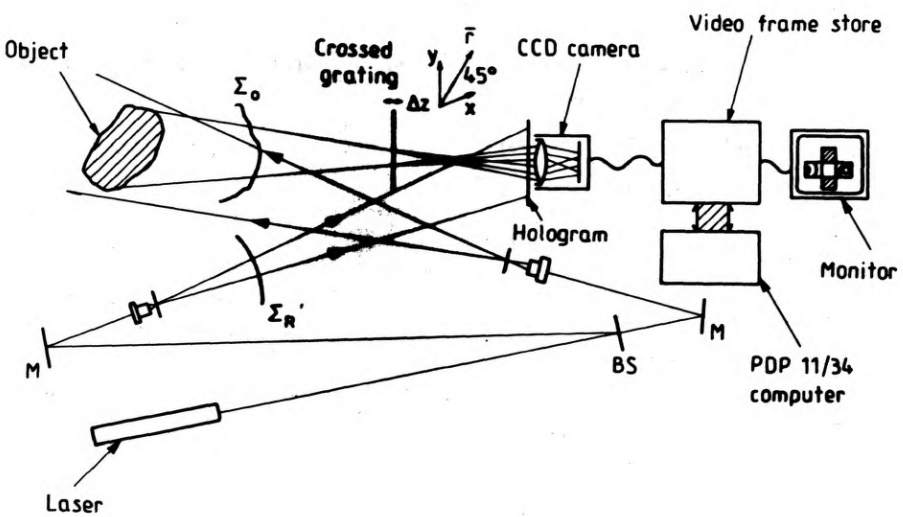


Fig 4. Holographic set-up producing four instantaneous interferograms. $\Sigma_o$, $\Sigma_R$ – object and reference beams, respectively, $M$ – mirrors, $BS$ – beamsplitter. If the linear grating is used in the set-up, the threechannel holographic interferometer is obtained

We present also another type of a fourchannel interferometer, i.e., the holographic, crossed-grating interferometer. Let us consider the set-up shown in Fig. 4. To obtain the information about the $x$ and $y$ direction slopes of the object a crossed-grating is applied. The holographic plate is illuminated by an object beam $\Sigma_o$ which passes through the diffraction grating. If we assume (for simplicity of considerations) a cosinusoidal profile of the sum-type grating, the wavefront

recorded on the hologram has the form

$$U(x,y) = O(x,y)\,T(x,y) = A(x,y)\exp(i\Phi(x,y))$$
$$[c_{0x}+c_{1x}\exp(i2\pi x)+c_{-1x}\exp(-i2\pi x)+c_{0y}+c_{1y}\exp(i2\pi y)+c_{-1y}\exp(i2\pi y)] \quad (11)$$

where $O(x,y)$ is the object beam with the amplitude $A(x,y)$ and the phase $\Phi(x,y)$, $c_{kx/y}$ (for $k = 0, \pm 1$) is the $k$-th coefficient of the one-dimensional Fourier series of a linear grating.

Let us assume that in a real-time holographic arrangement the object beam has not changed and the grating is translated along the optical axis, perpendicular to its plane. The longitudinal translation of the grating causes lateral-shear between the four first diffraction order wavefronts reconstructed from the hologram and the relevant object beams diffracted on the grating. Figure 5 shows the shift of an image

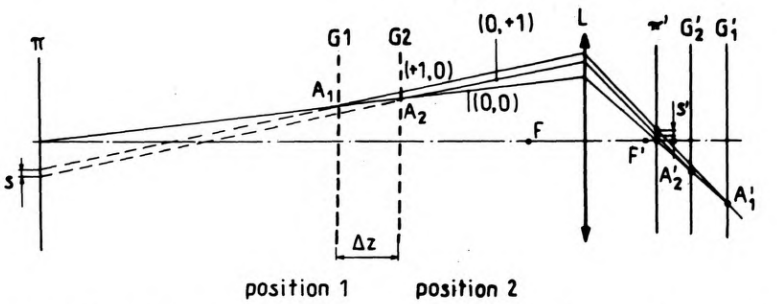


Fig. 5. Optical configuration of the object beam in the crossed-grating holographic interferometer ($s$, $s'$ – lateral shift of the first diffracted order image)

of an arbitrary object point introduced by the longitudinal translation of the grating. This results in the differentation of the wavefront in $x$ and $y$ directions. If we additionally introduce the adequate in-plane translation $r$ of the grating, so as to give the resultant shift $\delta_{\pm 1x} = \delta_{\pm 1y} = \pm 45$ deg, the interferograms obtained will be of the form given by Eq. (8).

Of course, the multichannel holographic interferometry requires special attention to the multiplicity of the reconstructed images. Illuminating with the reference beam $\Sigma_R$ the hologram on which five object beams were recorded (as shown by Eq. (11)) yields thirty reconstructions. Five of them are conjugate reconstructions. The others are the primary reconstructions ($R^*O^x_{+1}, R^*O^x_{-1}, R^*O^y_{+1}, R^*O^y_{-1}, R^*O_0$) and twenty undesired cross-reconstructions. In a real-time holographic arrangement the hologram is illuminated by five object beams propagating behind the grating. The hologram may be considered as a high frequency diffraction grating, so due to its multibeam illumination 15 beams are obtained which may be marked $(k,l)$, where $k$ is the diffraction order from the grating and $l$ is the diffraction order from the hologram ($k,l = \pm 1, 0$). Four beams ($\pm 1_x$, 0), ($-1_x$, 0), ($+1_y$, 0), ($-1_y$, 0) together with adequate self-reconstructions from the hologram give rise to the required interferograms. The other beams propagate in the same directions as some of the cross-reconstructions from the hologram and may form unwanted fringe patterns.

However, usually the intensity level in the noise fringe patterns is several times lower than in the analysed interferograms. Also the average spatial frequency of the hologram is usually much higher than that of the diffraction grating (here $f_G = 200$ 1/mm). Therefore the useful and noise beams propagate in different directions and the fringe patterns formed do not overlap.

For proper registration of the data the spatial frequency of the grating has to be sufficiently large to ensure the separation of the pupils obtained for the first diffraction orders and the zero diffraction order, i.e., $\Theta_G \geqslant a_o$ (where $a_o$ is the angular size of the object and $\Theta_G$ is the angle of the first diffraction order of the grating). If a product grating is used in the set-up the additional fringe patterns will occur (as shown in Fig. 3) due to beat frequencies. However the previous condition is sufficient to avoid overlapping with the first diffraction order images.

The processing of the information provided by the four fringe patterns causes additional problems which are discussed in Sections 4.2 and 5.2.

## 4. Data analysis

A general purpose image processing system is used for fringe pattern recording and analysis [9]. The system consists of a TV digitiser and frame store, controlled by a PDP 11/34 minicomputer. The frame store is configured to sample the video signal into $768 \times 586 \times 6$ bit pixels filling the rectangular video.

### 4.1. Threechannel interferometer

The fringe patterns from the 3 grating orders occupy $3 \times 256 \times 256$ square areas, side by side in the upper part of the image field. The remaining frame store memory is used to store a phase angle look-up table and the processed phase maps.

Software, previously developed for 3-phase step holographic fringe analysis [9], was adapted to convert the 3-fringe patterns to a map of phase (phase fringes or "wrapped" phase) using the solution given in Eq. (6) [5]. A phase angle look-up table is used to increase the processing speed. Due to the limitted size of the frame store memory, the look-up table was computed to 7 bit accuracy only (the maximal accuracy of the phase measurement $= 2.8$ deg). The hole in the look-up table represents the area within which the fringe contrast in the interferograms is too low for valid phase measurement. The $2\pi$ phase discontinuities which derive from the discontinuities in the $\tan^{-1}$ function are removed by a fringe counting or phase "unwrapping" procedure [10].

Figure 6 shows the result of the analysis of the computer generated interferograms (Fig. 6**a**–**c**) obtained with phase steps $-120$, 0, $+120$ deg, respectively. The data is processed using the software for analysis of real interferograms by replacing the data capture routine to evaluate Eq. (2). After processing the data with a threshold level shown at the look-up table (Fig. 6**e**), the wrapped (Fig. 6**f**) and unwrapped phase (Fig. 6**d**) are obtained. The intensity in Fig. 6**d**, **f** is proportional to

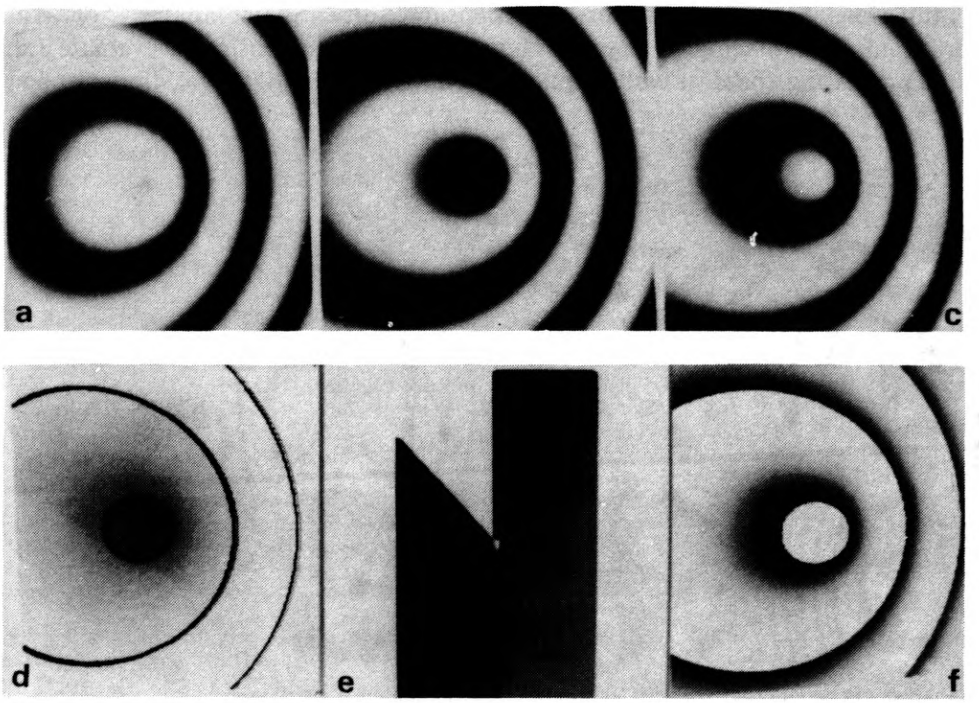


Fig. 6. Analysis of computer-generated interferograms (the threechannel interferometer). **a–c** – interferograms with the phase shift $-120$, 0, $+120$ deg, respectively; **d** – unwrapped and **f** – wrapped phase; **e** – look-up table

the phase values. The values have been scaled to cover the measured range of the phase variations. A dark overlay in Fig. 6**d** shows where fringe crossings have occurred.

### 4.2. Fourchannel interferometer

The four fringe patterns from 4 grating orders ($\pm 1_x$, $\pm 1_y$) occupy $4 \times 256 \times 160$ rectangle areas localized as shown in Fig. 7**a–d**. The remaining frame store memory is used to store the processed phase maps (the wrapped and unwrapped maps of phase $\Phi_x$ and $\Phi_y$ are shown in Fig. 7**e, f** and Fig. 7**g, h**, respectively).

The software was developed to convert the four fringe patterns to maps of phase $\Phi_x$ and $\Phi_y$ ("wrapped" phase) using the solution given in Eq. (9). The value of the phase is evaluated for each point and compared with the chosen threshold level and the area within which the fringe contrast in the interferograms is too low for valid phase measurement ("flag red"). The $2\pi$ phase discontinuities are removed by a fringe counting procedure [10]. Additionally the filtering procedure to remove some of the "red" peaks and areas and to smooth the functions is available at two stages: on the wrapped and unwrapped phase maps.

Figure 7 shows the result of the analysis of the computer generated interferograms (Fig. 7**a–d**) obtained with the phase shifts $\pm 45$ deg for $\Phi_x$ and $\Phi_y$

phase functions. The data is processed using software to analysis of real interferograms by replacing the data capture routine with a routine to evaluate Eq. (8). After processing the data with a manually chosen threshold level, the wrapped

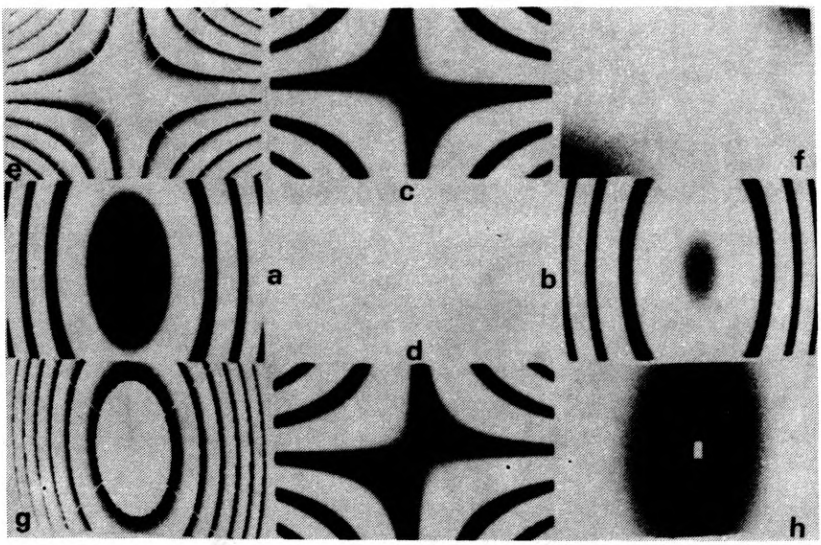


Fig. 7. Analysis of computer-generated interferograms (the fourchannel interferometer), **a–d** – interferograms with the phase shift $\pm 45$ deg in $x$ and $y$ directions, **e, f** – the unwrapped and wrapped phase $\Phi_y$, **g. h** – unwrapped and wrapped phase $\Phi_x$

(Fig. 7**f, h**) and unwrapped (Fig. 7**e, g**) phase $\Phi_x$ and $\Phi_y$ are obtained respectively. The intensities in Fig. 7**f–g** are proportional to the phase values and scaled to cover the measured range of phase variations.

## 5. Error analysis

The limitations in the determination of a phase function and the accuracy obtained in phase-stepping techniques have been discussed by many authors [11–13]. In multichannel phase-stepped interferometry we avoid several errors due to relative intensity changes and statistical fluctuations of the phase differences between the interfering beams caused by thermal perturbations and mechanical instabilities which occur during sequential acquisition of interferograms.

However, we have to consider additional sources of errors that are mainly due to the fact that the three or four interferograms are recorded from different parts of the detector or by different cameras. Also the mean intensity of the interferograms produced by different diffraction order beams may differ. In this technique it is impossible to improve the accuracy of the measurements by increasing the number of measurements. Therefore, especially in fourchannels interferometers, the areas within which the fringe contrast is too low for valid phase measurement enlarge due to systematic errors occuring in the set-up.

The possible additional sources of errors are as follows:

*Phase errors.*

– inaccuracy of the phase step (caused by inaccuracy in the translation of the grating),

– pixel mismatch (the proper definition of the image separation in pixels and the correct adjustment of the grating),

– distortion of the detector or the imaging optics;

*Intensity errors*

– different man intensity of the interferograms,

– different sensitivity of the relevant pixels in the three interferograms,

– electronic noise and non-linearity of the detector.

Herein we consider the systematic errors. The statistical error as a function of the intensity and phase functions is given by the equation [12]

$$(\delta\Phi)^2 = (2/3m^2)\,(\Delta I/I^2)+(1/2)\,(\Delta\Phi_k)^2 \tag{12}$$

where: $m$ is the fringe contrast, $\Delta I/I$ – the relative fluctuations of the intensities, $\Delta\Phi_k$ – the statistical fluctuations of the relative phases. The systematic errors will generally be periodic. Equation (12), however, is still valid for the rms value of the periodic phase error.

In order to evaluate the infleunce of the different sources of errors the interferograms are generated by computer. The general form of the intensity $I_k(x, y)$, at any point of the $k$–th interferogram is given by equation

$$I_k(x,y) = a_k(x,y)+b_k(x,y)\cos[\Phi(x,y)+\Phi_k+\Psi_k(x,y)] \tag{13}$$

where $a_k(x,y)$ is the background level which may change according to the diffraction efficiency of the grating, $b_k(x,y)$ is the contrast in the $k$-th interferogram, $\Psi_k(x,y)$ is the distortion of the detector or/and imaging optics. In fourchannel interferometer $\Phi(x,y)$ has the form of $\Phi_x$ or $\Phi_y$ functions in the adequate interferograms. Additionally the pixel mismatch in the $k$-th interferogram may be introduced by considering the intensities $I_k(x,y)$ with the co-ordinate shift $(x-\Delta x_k)$ and/or $(y-\Delta y_k)$.

An example of the basic solution for the data generated without an additional error function is shown in Figs. 6 and 7 for three- and fourchannel interferometers, respectively.

### 5.1. Errors in a threechannel interferometer

The systematic errors listed above generate quasi-periodic errors in the calculated phase map. They were studied carefully by the author in [5]. Herein we will summarize their influence on the results obtained.

All the phase errors cause a quasi-sinusoidal error that has twice the spatial frequency of the interference fringes. Figures 8–10 show the one-dimensional plots of the difference $\Delta\Phi$ between theoretical phase values and the values obtained by processing the data with various error function introduced. The inaccuracy in the phase steps generates sinusoidal error with approximatelly constant amplitude in

whole analysed area. The amplitude of the error function is of the same order as the errors of the phase step. Figure 8 shows the graph of the phase error when the shift is supposed to be 120, but is actually 115 deg.

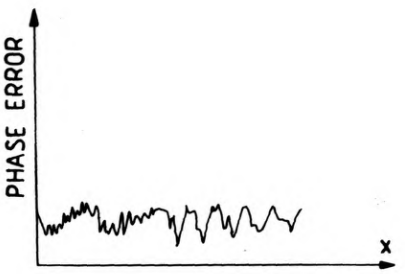


Fig. 8. Diagram of the phase error introduced by the phase shift inaccuracy 5 deg

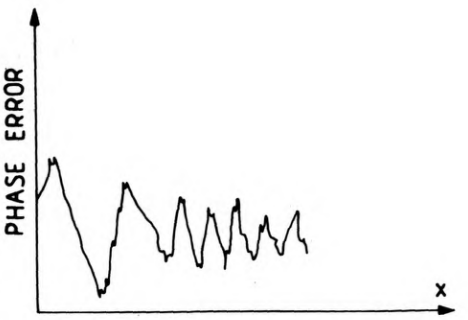


Fig. 9. Diagram of the phase error caused by the pixel mismatch in $x$ direction introduced for $\pm 1$ diffraction order interferograms

In order to match data in all three interferograms imaged at different areas of the detector, it is necessary to determine exact image separation and avoid rotation of the images with respect to the detector lines. If misalignment between pixels occurs, a shearing error is superimposed on the measured result. It may be interpreted as an additional inaccuracy of the phase step but depending on the spatial frequency of the fringes. Therefore the amplitude of the error in the plot shown in Fig. 5 decreases rapidly at the left part of the plot. If the minimum fringe period, given in pixels, is $p_{\min}$, the maximum pixel mismatch $\Delta p$ which will still enable correct fringe counting is given by relation

$$\Delta p = 1/4\, p_{\min}. \tag{14}$$

The additional phase given by the distortion of the detector and/or imaging optics, $\Psi_k(x, y)$, cause a systematic change in the phase shift at every point at the detector. Usually, in the central part of the detector ($k = 0$) the distortion function may be negligible, however at the outer part ($k = \pm 1$), it must be taken into account. Figure 10 shows the diagram of the phase error obtained from the analysis of the

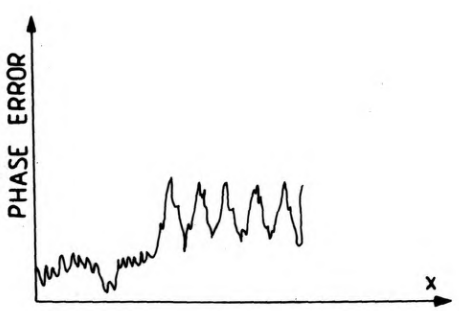


Fig. 10. Diagram of the phase error caused by the distortion function introduced in $\pm 1$ diffraction order interferograms

input interferograms with an additional distortion function. The amplitude of the quasi-sinusoidal error increases in proportion to the value of the distortion introduced.

The systematic intensity errors are due to the differences in the mean intensities in the analysed interferograms. If special care is not taken in the production of the gratings, the differences in the mean intensities may reach 50%. It causes the change of the shape of the phase fringes and the quasi-sinusoidal error with the same spatial frequency as the interference fringes analysed. Figure 11a shows the wrapped phase map obtained for 50% intensity differences between $\pm 1$ and 0-th diffraction order interferograms. The overlay in Fig. 11 shows the shape of the phase fringes and the phase error function at the middle line of the maps.

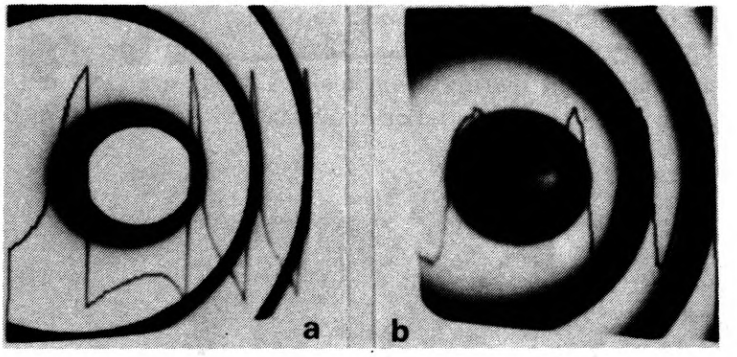


Fig. 11. Wrapped phase map (**a**) and the phase error map (**b**) obtained for 50% mean intensity differences between +1 and 0 diffraction order interferograms. The one-dimensional plots show the shape of the wrapped phase and phase error functions at the middle line of the maps

As the calculation of the interference phase is based on the simultaneous measurements of intensity given different pixels of the detector, the difference in sensivities of the relevant pixels of the detector, causes a statistical error. Also the detector introduces intensity measurement errors due to electronic noise and nonlinear response. The rms value of statistical error given by the variations of intensity equals

$$(\delta\Phi)^2 = (2/3m^2)\,(\Delta I/I)^2. \tag{15}$$

This error generally has a larger influence on the accuracy than in the case of sequential data aquisition.

### 5.2. Errors in a fourchannel interferometer

The source of errors in the fourchannel interferometer are very similar to those in the threechannel interferometer, although their influence on the accuracy of the results is more severe. It is due to minimal number of the phase steps introduced and the interacting between the functions $\Phi_x$ and $\Phi_y$.

In the phase-stepping techniques usually the maximum values of errors are obtained for the values of the phase 0 or $n\pi$ and nearby values. This is caused by the character of the tangent function. The error will be strongly enlarged, if both of the functions $\Phi_x$ and $\Phi_y$ tend to zero together. In order to enable fringe counting process in the whole analysed area we have to prevent division by zero in the relations

$$\tan\Phi_x = S_x/C_x \quad \text{and} \quad \tan\Phi_y = S_y/C_y$$

(where $S_x$, $S_y$ and $C_x$, $C_y$ are numerator and denominator in Eq. (9)) by putting the threshold $C_o$ for all areas where $C_x < C_o$ and $C_y < C_o$. The same threshold level is given to avoid the ambiguity where $S_x$, $C_x$ or $S_y$, $C_y$ reach together small values. In this way we obtained the "flag red" area. It shows how the phase fringes $\Phi_x$ break through into the wrapped map $\Phi_y$ and in the opposite. If no errors are introduced in the set-up, the high quality phase fringes are obtained and there are no problems with the fringe counting process (as shown in Fig. 7). If the errors occur, the threshold level has to be increased and the uncertain regions which are "flag red" occupy large areas as shown in Fig. 12**e**, **g** (the one pixel mismatch is introduced in $x$ and $y$ directions).

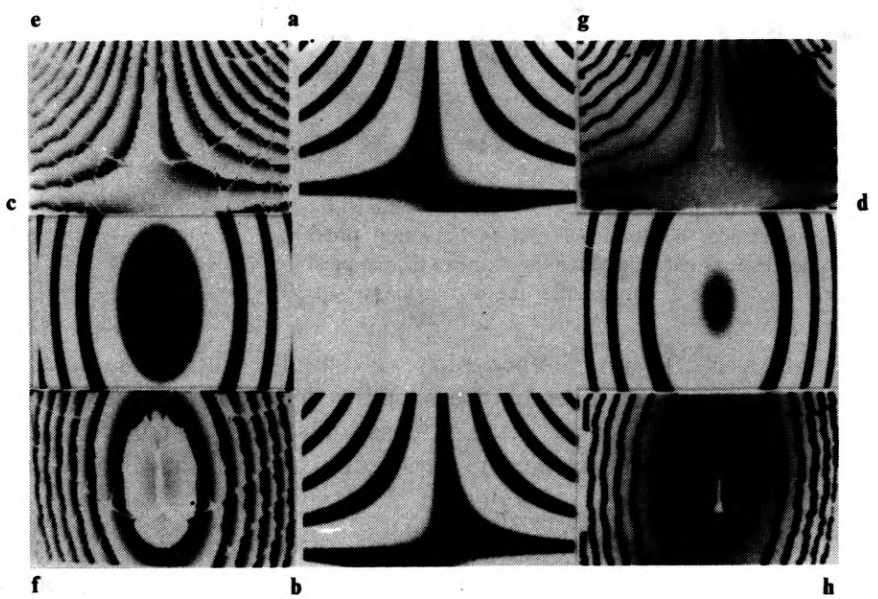


Fig. 12. Analysis of computer-generated interferometer with 1 pixel mismatch introduced in $x$ and $y$ directions. **a–d** – analysed interferograms, **e**, **g** – wrapped, and **f**, **h** – unwrapped phase maps of $\Phi_y$ and $\Phi_y$ functions, respectively

Herein to enable the phase unwrapping process the filtering has to be applied. The result of the phase unwrapping after filtering procedure is shown in Fig. 12**c**, **d**. However the filtering causes additional systematic error which has its maximum values at the phase jumps at the wrapped phase map, as shown in Fig. 13. In general, in the case of the filtering process introduced, the phase error maps (Fig. 14, 15) may be considered as the sum of errors caused by filtering and other sources of systematic

errors. Figure 14 shows the phase error maps (for both $\Phi_x$ and $\Phi_y$ functions) obtained by introducing the unaccuracy of phase shift (2 deg) – Fig 14**a**, **b**, one pixel mismatch in $x$ and $y$ directions – 14 **c**, **d** and the distortion function – Fig. 14**e**, **f**. The error functions have quasi-periodic character and have their extremal values along the

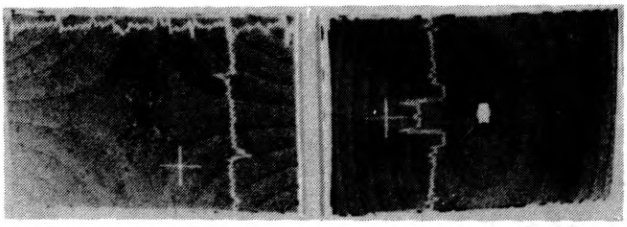

Fig. 13. Phase error maps obtained after processing the data shown in Fig. 6 and due to the filtering process performed on the wrapped phase

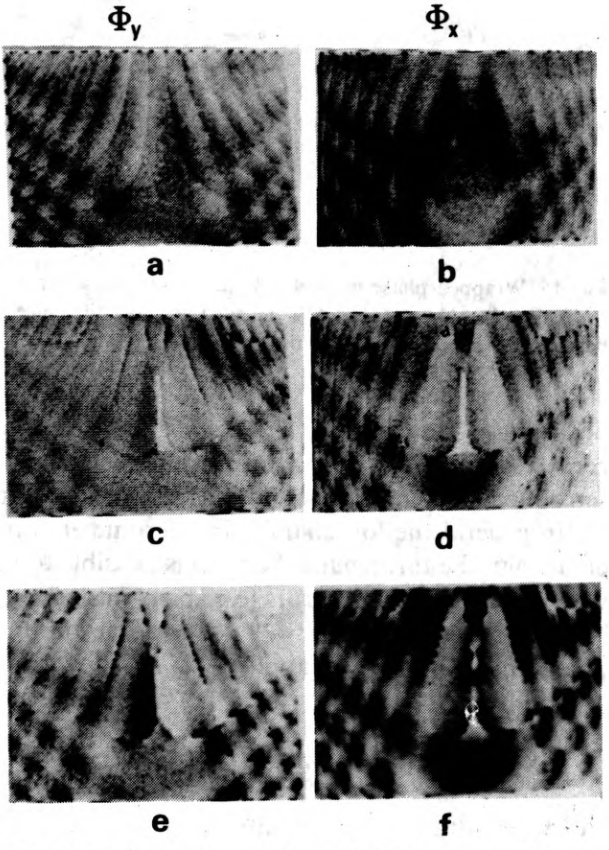


Fig. 14. Phase error maps obtained when the phase shift error is 2 deg (**a**, **b**), for the interferograms with 1 pixel mismatch in $x$ and $y$ directions (**c**, **d**), and for the interferograms with a distortion function introduced (**e**, **f**)

geometrical places where the phase fringes $\Phi_x$ break into the phase fringes $\Phi_y$. The character of the error maps for both functions $\Phi_x$ and $\Phi_y$ is very similar, although the error fringes are shifted in both cases.

The influence of the intensity errors is quite severe. The 5% difference of intensity in $\pm 1_x$ and $\pm 1_y$ diffraction order interferograms causes big errors in wrapped phase as shown in Fig. 15. The problem of large uncertain regions is especially severe when

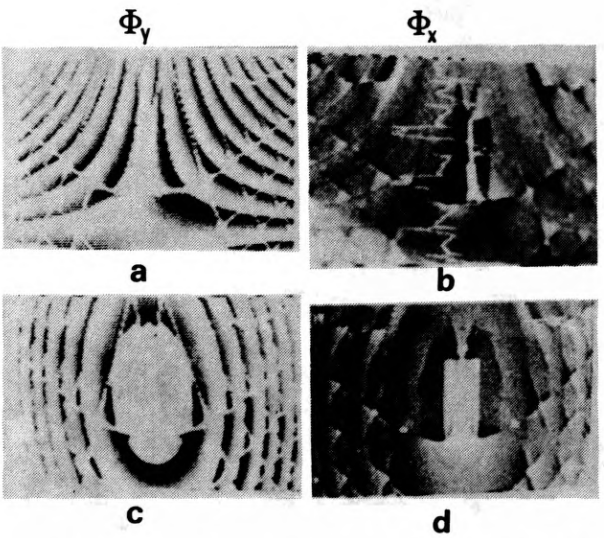


Fig. 15. Wrapped phase maps $\Phi_y$, $\Phi_x$ (**a**, **c**), and phase error maps (**b**, **d**) obtained for 5% mean intensity difference between $\pm 1_x$ and $\pm 1_y$ diffraction orders

both phase functions $\Phi_x$ and $\Phi_y$ (e.g., functions with rotational symmetry) tend to zero together [14]. During experiment this problem may be overcome by introducing an additional tilt in $x$ or/and $y$ directions.

In general the fourchannel interferometer is much more sensitive to any type of error than the threechannel one. It is possible to obtain reliable results from the data with reasonable small errors (e.g., pixel mismatch $\Delta p_{x/y} = 1$, differences of intensities $\sim 2\%$ or the distortion $\sim 1\%$), however the filtering procedure for the wrapped phase maps has to be applied.

## 6. Experimental results

To demonstrate the capability of the multichannel grating phase-stepped interferometers, we show experimental results obtained in threechannel holographical interferometer and fourchannel double-grating interferometer.

In the first case, the three interferograms are obtained in the set-up shown in Fig. 4. However, here we apply a linear grating which, after recording of the hologram, is

translated in-plane, only in the direction perpendicular to its grooves. This type of the threechannel holographic interferometer is explained in details in [5].

The special adjustment procedure is applied to determine the constant background illumination factor and the multiplication factor (for $\pm 1$ diffraction order beams). Pixel match in the interferograms is checked by correlating two ($+1$ or $-1$ with 0) diffraction order interferograms obtained after introducing changes in the object, but before translation of the grating. Two parameters have to be checked in this procedure: the value of the image separation in pixels and the correct adjustment of the grating. Although this adjustment needs careful attention, it has to be performed once for any given arrangement of the camera and grating. Later, any object or a transient event may be tested. After the adjustment procedure, a grating shift ($x_o = d/3$, $d = 0.005$ mm) is introduced and the fringe patterns obtained are converted to maps of phase difference using the data processing system described in Section 4.1. Figure 16 shows the three interferograms analysed and the resultant

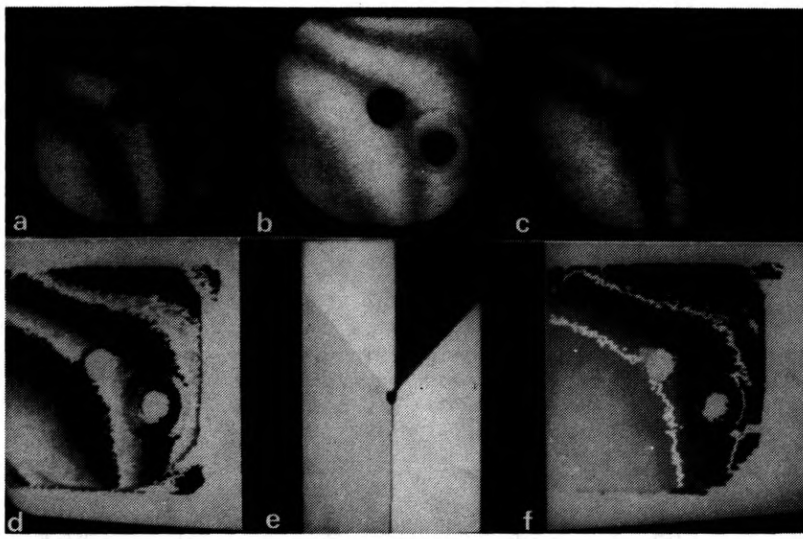


Fig. 16. Interferograms obtained simultaneously in a real-time threechannel holographic interferometer (**a–c**), wrapped and unwrapped phase maps (**d, f**), and look-up table (**e**)

wrapped and unwrapped phase maps. The measurements are performed so as to minimize most of the systematic errors, however the accuracy of phase step is low ($\sim 10\%$) and the system is not corrected for the distortion of the detector and imaging optics.

In the second case, the four interferograms containing information about the first derivatives of the wavefront in $x$ and $y$ directions are obtained in the double crossed-grating interferometer (as shown in Fig. 3). In order to apply the adjustment procedure similar to that described above, the gratings are positioned to obtain 0 phase shift between the interferograms. The constant background illumination factor

and multiplication factor between $x$ and $y$ direction interfeorgrams are checked. Also the pixel match in the interferograms is checked by correlating $+1$ and $-1$ diffraction orders in both directions. The pixel match between interferograms obtained from vertical and horizontal component grating is assured by the grating

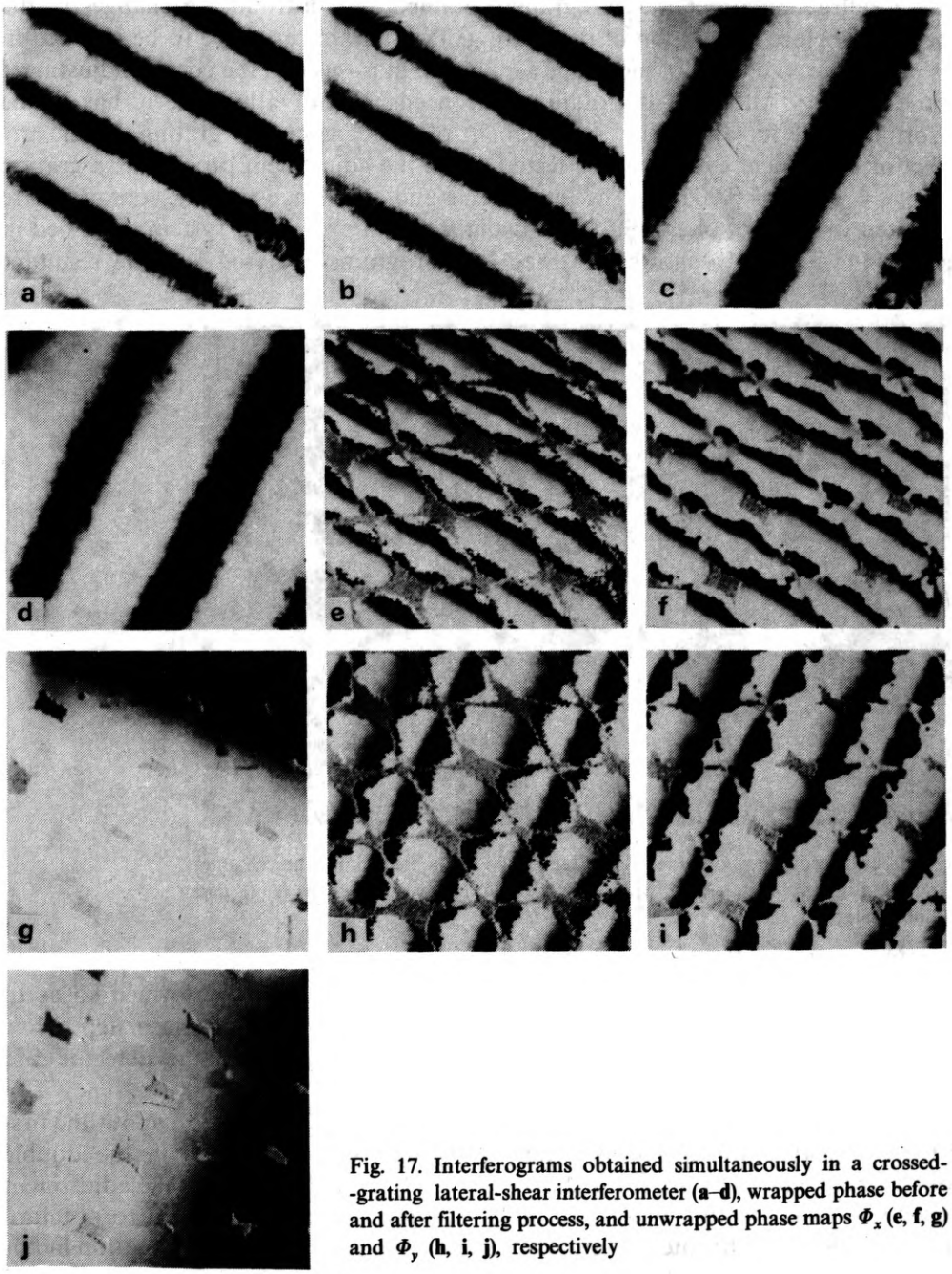


Fig. 17. Interferograms obtained simultaneously in a crossed--grating lateral-shear interferometer (a–d), wrapped phase before and after filtering process, and unwrapped phase maps $\Phi_x$ (e, f, g) and $\Phi_y$ (h, i, j), respectively

itself ($\omega_x = \omega_y$ and $\bar{\omega}_x^0 \perp \bar{\omega}_y^0$, where $\bar{\omega}_{x/y}^0$ is the versor of the component grating frequency).

After the adjustment procedure, a grating shift ($r = \frac{d}{2}\sqrt{2}$) is introduced in the 45 deg direction to the grooves of the grating and the four interferograms are captured simultaneously by the CCD camera. Figure 17**a–d** shows the four interferograms analysed. The wrapped phase $\Phi_x$ and $\Phi_y$ maps without and with filtering applied are shown in Fig. 17**e, f** and **h, i**. The main source of the error in the set-up is the inaccuracy of the phase shift. The large uncertain areas are recognized, therefore the filtering process is necessary. The fringe counting routine as applied to the filtered data and the wrapped phase maps are obtained (Fig. 17**g, j**).

The accuracy of the adjustment in the three- and fourchannel intereferometers is similar. Comparing the results obtained from both systems, we notice that the fourchannel interferometer suffers from the high sensitivity for the systematic errors in the set-up. The accuracy of both types of interferometers will be increased if the distortion error is measured and introduced as a correction in the algorithm and if a piezo-electric translator is used to introduce the phase shift.

## 7. Conclusions

New applications of multichannel phase-stepped interferometry have been presented whereby automatic fringe analysis in grating interferometers can be performed when recording transient events. The simple modifications of several conventional interferometers enable quantitative analysis of many dynamic processes. However, some of the advantages of conventional sequentially stepped phase measurement are lost. An initial calibration of the detector and imaging optics is necessary for variations in sensitivity, pixel mismatch and spatial distortion. Also the field of view of the system is limited and additional geometrical conditions must be fulfilled.

The theoretical analysis and computer simulation show the additional difficulties connected with the analysis of two interacting functions in fourchannel interferometer. The additional filtering in this case is proposed and its influence on the accuracy of the results is presented. The high sensitivity for the systematic errors in fourchannel interferometer is emphasized.

However, where quantitative metrology of transient events is important these disadvantages may be outweighed. Both theoretical and experimental results, which indicate the major limitation can be overcome, have been presented. Particular attention must be paid to the production of a high quality grating with near equal diffraction efficiency in the orders $\pm 1$, 0 (the threechannel interferometer) and the accurate initial adjustment of the grating, imaging optics and detector. The accuracy of the phase steps should be improved by using a piezo-electric translator. Further modifications of several conventional interferometers to convert them into multichannel phase-stepped interferometers are possible.

*Acknowledgements* – The author is grateful to the National Physical Laboratory and Dr D.W. Robinson for providing the software for the phase stepping method of fringe pattern analysis. Thanks are also due to the British Council for a Visiting Research Fellowship at NPL in the academic session 1986/87.

## References

[1] TIZIANI H. J., SPIE **599** (1985), 2.
[2] REID G. T., Opt. Lasers Eng. **7** (1986/87), 37 (and references therein).
[3] SCIAMMARELLA C. A., AHMADSHAI M. A., *Proc. of the VIIIth Int. Conf. on Exp. Stress Analysis*, Ansterdam, May 1986, 359.
[4] KWON O. Y., SHOUGH D. M., SPIE **599** (1985), 273.
[5] KUJAWIŃSKA M., ROBINSON D. W., *Multichannel phase-stepped holographic interferometry*, (submitted to Appl. Opt.).
[6] WYANT J. C., Appl. Opt. **12** (1973), 2057.
[7] KUJAWIŃSKA M., *Development of the theory of quasi-periodic diffraction grating systems*, (submitted to J. Opt. Soc. Am.).
[8] KUJAWIŃSKA M., *Fresnel field analysis of double grating systems and their application in phase stepping grating interferotemeters*, (submitted to J. Opt. Soc. Am.).
[9] ROBINSON D. W., Appl. Opt. **22** (1983), 2169.
[10] ROBINSON D. W., WILLIMAS D. C., Opt. Comm. **57** (1986), 26.
[11] SCHWIDER J., et al., Appl. Opt. **22** (1983), 3421.
[12] DANDLIKER R., THALMANN R., Opt. Eng. **24** (1985), 824.
[13] CHENG Y., WYANT J. C., Appl. Opt. **24** (1985), 3049.
[14] KUJAWIŃSKA M., *Application of phase-stepping automatic fringe analysis in moiré interferometry*, (submitted to Appl. Opt.).

*Received June 1, 1987*

## Многоканальные интерферометры с фазово-уступчатой сеткой

Предложено применение трёх- и четырёхканальных сеточных интерферометров для автоматического анализа линейных образов при исследовании быстро изменяющихся процессов. Представлены теоретические основы одновременного получения трёх и четырёх интерферограмм со сдвигом по фазе. С помощью компьютерной имитации проведён анализ источников ошибок. Продискутированы главные проблемы, связанные с анализом интерферограмм в четырёхканальном интерферометре. Представлена процедура юстирования таких интерферометров. Полученные экспериментальные результаты подтвердили полезность обсуждаемых систем.